Article

Elucidation of Fragmentation Mechanisms of Protonated Peptide Ions and Their Products: A Case Study on Glycylglycylglycine Using Density Functional Theory and Threshold Collision-Induced Dissociation

Houssain El Aribi, Christopher F. Rodriquez, David R. P. Almeida, Yun Ling, William W.-N. Mak, Alan C. Hopkinson, and K. W. Michael Siu

J. Am. Chem. Soc., **2003**, 125 (30), 9229-9236• DOI: 10.1021/ja0207293 • Publication Date (Web): 04 July 2003

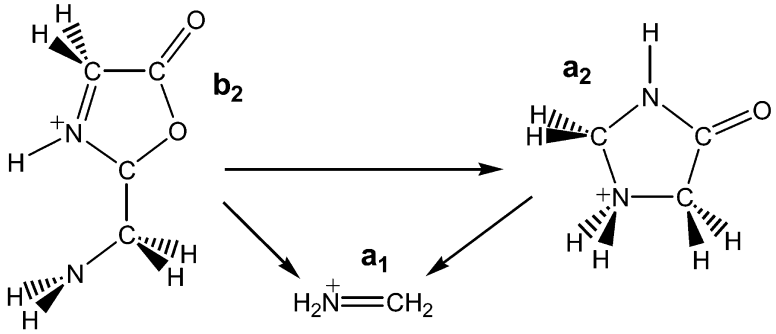

More About This Article

Additional resources and features associated with this article are available within the HTML version:

- Supporting Information
- Links to the 7 articles that cite this article, as of the time of this article download
- Access to high resolution figures
- Links to articles and content related to this article
- Copyright permission to reproduce figures and/or text from this article

View the Full Text HTML

J|A|C|S
ARTICLES
Published on Web 07/04/2003

Elucidation of Fragmentation Mechanisms of Protonated Peptide Ions and Their Products: A Case Study on Glycylglycylglycine Using Density Functional Theory and Threshold Collision-Induced Dissociation

Houssain El Aribi,[†] Christopher F. Rodriquez,[†,‡] David R. P. Almeida,[†] Yun Ling,[†,§] William W.-N. Mak,[||] Alan C. Hopkinson,[†] and K. W. Michael Siu*,[†]

Contribution from the Department of Chemistry and Centre for Research in Mass Spectrometry, York University, 4700 Keele Street, Toronto, Ontario, Canada M3J 1P3, and Biotechnology Centre for Applied Research and Training, Seneca at York, Seneca College, 70 The Pond Road, Toronto, Ontario, Canada M3J 3M6.

Received May 23, 2002; E-mail: kwmsiu@yorku.ca

Abstract: The fragmentation mechanisms of protonated triglycine and its first-generation dissociation products have been investigated using a combination of density functional theory calculations and threshold collision-induced dissociation experiments. The activation barrier measured for the fragmentation of protonated triglycine to the b_2 ion and glycine is in good agreement with a calculated barrier at the B3LYP/6-31++G(d,p) level of theory reported earlier [Rodriquez, C. F. et al. *J. Am. Chem. Soc.* **2001**, *123*, 3006−3012]. The b_2 ion fragments to the a_2 ion via a transition state structure that is best described as acylium-like. Contrary to what is commonly assumed, the lowest energy structure of the a_2 ion is not an iminium ion, but a cyclic, protonated 4-imidazolidone. Furthermore, fragmentation of the b_2 to the a_1 ion proceeds not via a mechanism that results in HNCO and $H_2C{=}C{=}O$ as byproducts, as have been postulated, but via a transition state that contains an incipient a_1 ion and an incipient carbene. The fragmentation of a_2 to a_1 proceeds via a transition state structure that contains the a_1 ion, CO and an imine as incipient components.

Introduction

Proton transport across hydrogen bonds has long been recognized as the mechanism through which many biological functions are carried out.[1] Proton tunneling or migration has been postulated to play a major role in the activity of adenosine triphosphate.[2] In protonated gas-phase ions, proton migration is the underlying feature of the "mobile-proton model" that drives the charge-directed nature of low-energy (<100 eV) peptide fragmentation and the heterogeneous nature of the fragmentation products.[3] However, the mechanism by which the proton migrates along a peptide backbone is not fully understood.[3−5] Details of this mechanism are required to develop insights into how peptides fragment; this has important applications in gas-phase microsequencing, a technology that become increasingly important for protein identification in proteomics.

In solution, the N-terminal amino nitrogen is the preferred protonation site of peptides that are devoid of basic residues, e.g., glycylglycylglycine (G_3). Thus, protonated G_3 that desorbs from solution must tautomerize to a heterogeneous population of fragmenting peptide isomers by transporting its ionizing proton. DFT calculations show that in vacuo the tautomer of protonated G_3 that has the lowest free energy is one in which the proton resides on the carbonyl oxygen of the first amide linkage and is hydrogen-bonded to the amino nitrogen atom.[5] Another tautomer, one in which the proton resides on the same carbonyl oxygen atom, but is hydrogen-bonded to the carbonyl oxygen atom of the second peptide linkage, is only 0.1 kcal/mol higher in free energy at the B3LYP/6-31++G(d,p) level of theory.[5] By contrast, the tautomer in which the proton resides on the N-terminal nitrogen atom contains two hydrogen bonds (one bridging an amino hydrogen with the carbonyl oxygen atom of the first peptide linkage and another bridging a second amino hydrogen with the carbonyl oxygen of the C-terminal carboxylic acid group) is 1.3 kcal/mol higher in free energy.[5] The barriers to interconversion between these tautomers are all smaller than 15 kcal/mol and are easily accessible under low-energy fragmentation conditions.[5] Thus, the proton is indeed "mobile" under low-energy CID conditions.

[†] York University.
[‡] Current address: Department of Chemistry, McNeese State University, 221D Kirkman Hall, 4205 Ryan Street, Lake Charles, LA 70609.
[§] Current address: Department of Chemistry, University of British Columbia, 2036 Main Mall, Vancouver, BC, Canada V6T 1Z1.
[||] Seneca College; current address: Genome Research Centre, University of Hong Kong, Pokfulam Road, Hong Kong.

(1) Bountis, T., Ed. *Proton Transfer in Hydrogen-Bonded Systems*; NATO ASI Series B.: Physics Vol. 291; Plenum Press: New York, 1992; pp 1−355.
(2) Senior, A. E. *Annu. Rev. Biophys. Biophys. Chem.* **1990**, *19*, 7−41.
(3) (a) McCormack, A. L.; Jones, J. L.; Wysocki, V. H. *J. Am. Soc. Mass Spectrom.* **1992**, *3*, 859−862. (b) Jones, J. L.; Dongre, A. R.; Somogyi, A.; Wysocki, V. H. *J. Am. Chem. Soc.* **1994**, *116*, 8368−8369. (c) Dongre, A. R.; Jones, J. L.; Somogyi, A.; Wysocki, V. H. *J. Am. Chem. Soc.* **1996**, *118*, 8365−8374. (d) Dongre, A. R.; Somogyi, A.; Wysocki, V. H. *J. Mass Spectrom.* **1996**, *31*, 339−350.
(4) Rodriquez, C. F.; Cunje, A.; Shoeib, T.; Chu, I. K.; Hopkinson, A. C.; Siu, K. W. M. *J. Phys. Chem. A* **2000**, *104*, 5023−5028.
(5) Rodriquez, C. F.; Cunje, A.; Shoeib, T.; Chu, I. K.; Hopkinson, A. C.; Siu, K. W. M. *J. Am. Chem. Soc.* **2001**, *123*, 3006−3012.

10.1021/ja0207293 CCC: $25.00

Fragmentation of a protonated peptide typically produces one charged product (the product ion) and one neutral fragment.[6] If fragmentation occurs at the C−N bond of a peptide linkage, and if the charge is retained on the N-terminal fragment, a *b* ion is produced; if the charge is retained on the C-terminal fragment, a *y* ion is produced after proton migration from the N-terminal to the C-terminal product. Other product ions, including the *a* ions, internal iminium (immonium) ions (that originate from nonterminal residues) and ions that result from the loss of small neutral molecules, e.g., CO, H_2O, and NH_3, may also be formed from the fragmentation of the protonated peptide or from its charged products. For many years, *b* ions were thought to be acylium ions.[6] Pioneering work by the Harrison group[7] has established that, at least for peptides that have residues containing alkyl side chains, the b_2 ion is a protonated oxazolone. For peptides containing residues that bear functional groups which can participate in cyclization reactions, competing reactions can take place and alternative b_2 ion structures have been proposed.[8−11] The *a* ions are believed to be iminium ions;[6] it will be shown in this study that this is not correct, at least for the a_2 ion of peptides that contain only alkyl side chains (vide infra). The *y* ions are believed to be protonated truncated peptides.[7c,8] As discussed earlier, the mechanisms by which most of these fragment ions are formed are either unknown or poorly understood. Present results suggest that many of the mechanistic details previously proposed[12] are probably incorrect.

To complement CID methods, a number of tools have been employed to probe the chemistry of protonated peptides in the gas phase; these include surface-induced dissociation,[13−22] ion mobility techniques,[23] blackbody infrared radiative dissociation,[24,25] and kinetic techniques.[26] A first step in elucidating fragmentation chemistry is to know the activation barriers of the various dissociation processes. Documented attempts have had mixed success.[26,27] Klassen and Kebarle[27c] employed threshold CID measurements in measuring activation barriers of the fragmentation of protonated glycine, diglycine, and triglycine and their derivatives. Their primary objective was to examine the fragmentation chemistries of protonated peptides. For protonated glycine and diglycine, this objective was met as these ions were relatively small and the kinetic shifts (vide infra) associated with their fragmentation were not too large to make their measurements suspect. Vibrational frequencies needed in the modeling (vide infra) were calculated at HF/3-21G or AM1. For protonated triglycine, no kinetic shifts, and thus no activation barriers, were provided because these were judged to be unreliable, in view of the estimated extent of the shifts and the use of MNDO, a low-level semiempirical method, for geometric optimization and vibrational frequency calculations.

Here we report results of a detailed experimental and theoretical investigation on the dissociation of ions generated from protonated G_3, in particular, the mechanisms of the following fragmentation reactions: protonated G_3 to b_2, b_2 to a_2, b_2 to a_1, and a_2 to a_1 ions. The experimental approach is threshold CID, coupled with vibrational frequencies and rotational constants derived from DFT calculations at the B3LYP/6-31++G(d,p) level of theory. These calculations also provide the energetics of the minima and transition state structures, from which reaction profiles can be constructed and activation barriers calculated.

Computational Method

Calculations were performed using Gaussian 98 [28] on a Silicon Graphics Origin 2000 with 16 processors and 8 GB of memory. DFT at the hydrid B3LYP level,[29] in conjunction with the 6-31++G(d,p) basis set,[28] was employed for structure optimizations and for the characterization of critical points using harmonic vibrational frequency calculations.[30] Estimated structures of the transition states were determined using the QST2 method.[28] First-order saddle points were then found using the Berny transition state algorithm and the CalcAll method.[28] Intrinsic reaction coordinate calculations were carried out to establish the minima associated with particular transition states.[28]

(6) Papayannopoulous, I. A. *Mass Spectrom. Rev.* **1995**, *14*, 49−73.
(7) (a) Yalcin, T.; Khouw, C.; Csizmadia, I. G.; Peterson, M. B.; Harrison, A. G. *J. Am. Soc. Mass Spectrom.* **1995**, *6*, 1164−1174. (b) Yalcin, T.; Csizmadia, I. G.; Peterson, M. B.; Harrison, A. G. *J. Am. Soc. Mass Spectrom.* **1996**, *7*, 233−242. (c) Nold, M. J.; Wesdemiotis, C.; Yalcin, T.; Harrison, A. G. *Int. J. Mass Spectrom. Ion Proc.* **1997**, *164*, 137−153.
(8) (a) Cordero, M. M.; Houser, J. J.; Wesdemiotis, C. *Anal. Chem.* **1993**, *65*, 1594−1601. (b) Reid, G. E.; Simpson, R. J.; O'Hair, R. A. J. *Int. J. Mass Spectrom.* **1999**, *190/191*, 209−230.
(9) Eckart, K.; Holthausen, M. C.; Koch, W.; Spiess, J. *J. Am. Soc. Mass Spectrom.* **1998**, *9*, 1002−1011.
(10) Farrugia, J. M.; O'Hair, R. A. J.; Reid, G. E. *Int. J. Mass Spectrom.* **2001**, *210/211*, 71−87.
(11) (a) Tsaprailis, G.; Nair, H.; Somogyi, A.; Wysocki, V. H.; Zhong, W.; Futrell, J. H.; Summerfield, S. G.; Gaskell, S. J. *J. Am. Chem. Soc.* **1999**, *121*, 5142−5154. (b) Tsaprailis, G.; Somogyi, A.; Nikolaev, E. N.; Wysocki, V. H. *Int. J. Mass Spectrom.* **2000**, *195/196*, 467−479.
(12) Ambihapathy, K.; Yalcin, T.; Leung, H.-W.; Harrison, A. G. *J. Mass Spectrom.* **1997**, *32*, 209−215.
(13) McCormack, A. L.; Somogyi, Á.; Dongré, A. R.; Wysocki, V. H. *Anal. Chem.* **1993**, *65*, 2859−2872.
(14) Wysocki, V. H.; Jones, J. L.; Dongré, A. R.; Somogyi, Á.; McCormack, A. L. *Biological Mass Spectrometry: Present and Future*; John Wiley and Sons Ltd: New York, 1994; Chapter 2.14, pp 249−254.
(15) Bier, M. E.; Schwartz, J. C.; Schey, K. L.; Cooks, R. G. *Int. J. Mass Spectrom. Ion Processes* **1990**, *103*, 1−19.
(16) Aberth, W. *Anal. Chem.* **1990**, *62*, 609−611.
(17) (a) Williams, E. R.; Henry, K. D.; McLafferty, F. W.; Shabanowitz, J.; Hunt, D. F. *J. Am. Soc. Mass Spectrom.* **1990**, *1*, 413−416. (b) Chorush, R. A.; Little, D. P.; Beu, S. C.; Wood, T. D.; McLafferty, F. W. *Anal. Chem.* **1995**, *67*, 1042−1046.
(18) Wright, A. D.; Despeyroux, D.; Jennings, K. R.; Evans, S.; Riddoch, A. *Org. Mass Spectrom.* **1992**, *27*, 525−526.
(19) Cole, R. B.; LeMeillour, S.; Tabet, J.-C. *Anal. Chem.* **1992**, *64*, 365−371.
(20) Schey, K. L.; Durkin, D. A.; Thornburg, K. R. *J. Am. Soc. Mass Spectrom.* **1995**, *6*, 257−263.
(21) (a) Laskin, J. Denisov, E.; Futrell, J. *J. Am. Chem. Soc.* **2000**, *122*, 9703−9714. (b) Laskin, J. Denisov, E.; Futrell, J. *J. Phys. Chem. B* **2001**, *105*, 1895−1900.
(22) (a) Wainhaus, S. B.; Gislason, E. A.; Hanley, L. *J. Am. Chem. Soc.* **1997**, *119*, 4001−4007. (b) Lim, H.; Schultz, D. G.; Gislason, E. A.; Hanley, L. *J. Phys. Chem. B* **1998**, *102*, 4573−4580. (c) Lim, H.; Schultz, D. G.; Gislason, E. A.; Hanley, L. *J. Phys. Chem. B* **1998**, *102*, 9362. (d) Lim, H.; Schultz, D. G.; Yu, C.; Hanley, L. *Anal. Chem.* **1999**, *71*, 2307−2317.
(23) Hoaglund-Hyzer, C. S.; Counterman, A. E.; Clemmer, D. E. *Chem. Rev.* **1999**, *99*, 3037−3079.
(24) (a) Dunbar, R. C. *J. Phys. Chem.* **1994**, *98*, 8705−8712. (b) Dunbar, R. C.; McMahon, T. B. *Science* **1998**, *279*, 194−197.
(25) (a) Price, W. D.; Schnier, P. D.; Williams, E. R. *Anal. Chem.* **1996**, *6*, 8, 859−866. (b) Price, W. D.; Schnier, P. D.; Jockusch, R. A.; Strittmatter, E. F.; Williams, E. R. *J. Am. Chem. Soc.* **1996**, *118*, 10 640−10 644.
(26) Vékey, K.; Somogyi, A.; Wysocki, V. H. *Rapid Commun. Mass Spectrom.* **1996**, *10*, 911−918.
(27) (a) Anderson, S. G.; Blades, A. T.; Klassen, J.; Kebarle, P. *Int. J. Mass Spectrom. Ion Processes* **1995**, *141*, 217−228. (b) Klassen, J. S.; Anderson, S. G.; Blades, A. T.; Kebarle, P. *J. Phys. Chem.* **1996**, *100*, 14 218−14 227. (c) Klassen, J. S.; Kebarle, P. *J. Am. Chem. Soc.* **1997**, *119*, 6552−6563.
(28) Frisch, M. J.; Trucks, G. W.; Schlegel, H. B.; Scuseria, G. E.; Robb, M. A.; Cheeseman, J. R.; Zakrzewski, V. G.; Montgomery, J. A., Jr.; Stratmann, R. E.; Burant, J. C.; Dapprich, S.; Millam, J. M.; Daniels, A. D.; Kudin, K. N.; Strain, M. C.; Farkas, O.; Tomasi, J.; Barone, V.; Cossi, M.; Cammi, R.; Mennucci, B.; Pomelli, C.; Adamo, C.; Clifford, S.; Ochterski, J.; Petersson, G. A.; Ayala, P. Y.; Cui, Q.; Morokuma, K.; Malick, D. K.; Rabuck, A. D.; Raghavachari, K.; Foresman, J. B.; Cioslowski, J.; Ortiz, J. V.; Stefanov, B. B.; Liu, G.; Liashenko, A.; Piskorz, P.; Komaromi, I.; Gomperts, R.; Martin, R. L.; Fox, D. J.; Keith, T.; Al-Laham, M. A.; Peng, C. Y.; Nanayakkara, A.; Gonzalez, C.; Challacombe, M.; Gill, P. M. W.; Johnson, B. G.; Chen, W.; Wong, M. W.; Andres, J. L.; Head-Gordon, M.; Replogle, E. S.; Pople, J. A. *Gaussian 98*, revision A.5; Gaussian, Inc.: Pittsburgh, PA, 1998.
(29) (a) Becke, A. D. *Phys. Rev.* **1988**, *A38*, 3098−3100. (b) Becke, A. D. *J. Chem. Phys.* **1993**, *98*, 5648−5652. (c) Lee, C.; Yang, W.; Parr, R. G. *Phys. Rev.* **1988**, *B37*, 785−789.

Table 1. Energies (hartrees) and Relative Energies (kcal/mol)

structure	E_t	E_{ZPVE}	$\Delta H°_0$	$H°_{298}$	$G°_{298}$	$S°$	$\Delta G°_{298}$
1	−416.367623	−416.246565	0.0	−416.238078	−416.278647	85.4	0.0
2	−416.326584	−416.211327	22.1	−416.199844	−416.250066	105.701	17.9
3	−303.0041565	−302.895247		−302.887538	−302.92637	81.728	
3 + CO	−416.3214795	−416.207552	24.5	−416.196539	−416.257813	128.928	13.1
4	−303.025573	−302.911627		−302.905236	−302.9405	74.2	
4 + CO	−416.342896	−416.223932	14.2	−416.214237	−416.271943	121.4	4.2
HNCO	−168.6913238	−168.67013		−168.665918	−168.693035	57.072	
H_2CCO	−152.6109362	−152.579378		−152.574903	−152.602994	59.122	
5	−416.286926	−416.179902	41.8	−416.167283	−416.247984	169.894	19.2
6	−416.3307136	−416.213567	20.7	−416.203527	−416.249764	97.315	18.1
7	−416.3438637	−416.227695	11.8	−416.218051	−416.262763	94.105	10.0
8	−416.3448198	−416.227711	11.8	−416.218145	−416.262814	94.015	9.9
9	−321.329003	−321.266344		−321.26084	−321.294276	70.4	
9 + $H_2N^+CH_2$	−416.313669	−416.196738	31.3	−416.187302	−416.246231	124.1	20.3
10	−321.662039	−321.586466		−321.580654	−321.614664	71.6	
10 + CH_2NH	−416.302848	−416.187343	37.2	−416.177666	−416.23746	125.9	25.8
11	−321.285258	−321.223071		−321.217393	−321.251106	70.954	
11 + $H_2N^+CH_2$	−416.269924	−416.153465	58.4	−416.143855	−416.203061	124.654	47.4
12	−302.993183	−302.883917		−302.876156	−302.914574	80.9	
12 + CO	−416.310506	−416.196222	31.6	−416.185157	−416.246017	128.1	20.5
13	−302.961036	−302.854207		−302.845428	−302.887477	88.501	
13 + CO	−416.278359	−416.166512	50.2	−416.154429	−416.21892	135.701	37.5
14	−302.989813	−302.888348		−302.877118	−302.927173	105.4	
14 + CO	−416.307136	−416.200653	28.8	−416.186119	−416.258616	152.6	12.6
15	−189.668871	−189.573803		−189.603435	−189.603435	77.6	
15 + 2CO	−416.303517	−416.198413	30.2	−416.221437	−416.266321	172	7.7
CO	−113.317323	−113.312305		−113.309001	−113.331443	47.2	
CH_2NH	−94.640809	−94.600877		−94.597012	−94.622796	54.3	
$H_2N^+CH_2$	−94.984666	−94.930394		−94.926462	−94.951955	53.7	
$H_2N^+CH_2$ + CH_2NH + 2CO	−416.260121	−416.155881	56.9	−416.141476	−416.237637	202.4	25.7
aziridinone	−207.94384	−207.893547		−207.888847	−207.919188	63.857	
$H_2N^+CH_2$ + aziridinone +CO	−416.245829	−416.136246	69.2	−416.12431	−416.202586	164.757	47.7
TS(1−2)	−416.311084	−416.194214	32.9	−416.184278	−416.229692	95.6	30.7
TS(3−4)	−302.985282	−302.877065		−302.869612	−302.90743	79.6	
TS(3−4) + CO	−416.302605	−416.18937	35.9	−416.178613	−416.238873	126.8	25.0
TS(1−5)	−416.244408	−416.132696	71.5	−416.121513	−416.172085	106.437	66.9
TS(1−6)	−416.2981187	−416.180388	41.5	−416.170853	−416.216021	95.065	39.3
TS(6−7)	−416.329421	−416.212233	21.5	−416.202923	−416.2469	92.556	19.9
TS(7−8)	−416.3433496	−416.229724	10.6	−416.22043	−416.264282	92.293	9.0
TS(4−12)	−302.9900136	−302.88099		−302.874067	−302.910597	76.884	
TS(4−12) + CO	−416.3073366	−416.193295	33.4	−416.183068	−416.24204	124.084	23.0
TS(3−14)	−302.958806	−302.854668		−302.845139	−302.889002	92.3	
TS(3−14) + CO	−416.276129	−416.166973	49.9	−416.15414	−416.220445	139.5	36.5

E_t = total electronic energy. E_{ZPVE} = total electronic energy corrected with zero-point vibrational energy. $H°_{298} = E_{ZPVE} + E_{vibrational} + E_{rotational} + E_{translational} + RT$ (T = 298 K). $G°_{298} = H°_{298} - TS°$ (T = 298 K). $S°$ in cal/mol K.

Previous investigations have established that DFT calculations at the B3LYP/6-31++G(d,p) level of theory perform satisfactorily for molecules, such as protonated peptides, in which hydrogen bonding is an important structural feature[4,5,31]. DFT calculations employing hybrid functionals such as B3LYP correctly and accurately describe this relatively weak, but important, bond that is responsible for many structural details of protonated peptides and their fragmentation products. Table 1 lists the calculated structures' total electronic energies (E_t), total electronic energies corrected with zero-point vibrational energies (E_{ZPVE} or $H°_0$), relative enthalpies at zero K ($\Delta H°_0$), enthalpies at 298 K ($H°_{298}$), free energies at 298 K ($G°_{298}$), entropies ($S°$), and relative free energies at 298 K ($\Delta G°_{298}$). Some slight error may be introduced in the calculation of the entropies, and hence free energies, by our adopting the usual assumption made in Gaussian that ions with low frequencies have simple harmonic vibrations.

Experimental Method

The experimental details were similar to those used in previous studies.[32] Threshold CID measurements were conducted on a PE SCIEX API III triple-quadrupole mass spectrometer (Concord, Ontario). Triglycine is commercially available from Sigma (St. Louis, MO); all chemicals were from Sigma and Aldrich (St. Louis, MO). Samples were 10 μM of glycylglycylglycine in 70/30 water/methanol containing 0.1% acetic acid. They were electrosprayed at a flow rate of 3 μL/min with air being the nebulizer gas. Ions thus formed were sampled from the atmospheric-pressure ion source into an "enclosed" quadrupolar lens region (q0), where multiple collisions with the "curtain-gas" molecules of nitrogen sampled with the ions occur. When needed, first-generation product ions, b_2 and a_2, were first produced in the region between the orifice and q0, and collisionally deactivated downstream. Extensive studies have shown that thermalization of the sampled ions in the lens region is highly efficient[33]—threshold energies determined with our apparatus using lens collision energies that were higher by 4−6 eV (laboratory frame) than those used in the actual determination (8−12 eV) were indistinguishable from those acquired under standard conditions. These data suggest strongly that thermalization of ions in our mass spectrometer is efficient and that the temperature of the ions that

(30) (a) Ditchfield, R.; Hehre, W. J.; Pople, J. A. *J. Chem. Phys.* **1971**, *54*, 724−728. (b) Hehre, W. J.; Ditchfield, R.; Pople, J. A. *J. Chem. Phys.* **1972**, *56*, 2257−2261. (c) Hariharan, P. C.; Pople, J. A. *Mol. Phys.* **1974**, *27*, 209−214. (d) Gordon, M. S. *Chem. Phys. Lett.* **1980**, *76*, 163−168. (e) Hariharan, P. C.; Pople, J. A. *Theor. Chim. Acta* **1973**, *28*, 213−222. (f) Clark, T.; Chandrasekhar, J.; Spitznagel, G. W.; Schleyer, P.v. R. *J. Comput. Chem.* **1983**, *4*, 294−301.

(31) (a) Rodriquez, C. F.; Shoeib, T.; Chu, I. K.; Siu, K. W. M.; Hopkinson, A. C. *J. Phys. Chem. A* **2000**, *104*, 5335−5342. (b) Shoeib, T.; Rodriquez, C. F.; Siu, K. W. M.; Hopkinson, A. C. *Phys. Chem. Chem. Phys.* **2001**, *3*, 853−861. (c) Addario, V.; Guo, Y.; Chu, I. K.; Ling, Y.; Ruggerio, G.; Rodriquez, C. F.; Hopkinson, A. C.; Siu, K. W. M. *Int. J. Mass Spectrom.*, **2002**, *219*, 101−114.

(32) (a) El Aribi, H.; Shoeib, T.; Ling, Y.; Rodriquez, C. F.; Hopkinson, A. C.; Siu, K. W. M. *J. Phys. Chem. A* **2002**, *106*, 2908−2914. (b) El Aribi, H.; Rodriquez, C. F.; Shoeib, T.; Ling, Y.; Hopkinson, A. C.; Siu, K. W. M. *J. Phys. Chem. A* **2002**, *106*, 8798−8805.

undergo collision-induced dissociation downstream is near 298 K. Collision-induced dissociation was performed mostly with argon as the neutral gas.[32] Xenon was also used initially; the modeled threshold curves at 0 K determined with Xe had larger slopes than those determined with Ar, and the threshold energies were typically smaller by < 0.1 eV. The plots were, however, more scattered. This, in combination with xenon's higher cost, resulted in our preference for argon. The gas pressure in q2 was continuously monitored with an upstream baritron gauge, the read out of which was converted into collision-gas thickness (CGT, the product of the neutral gas number density and the length of q2)[34] by the mass spectrometric software.

The threshold energy for the CID of a given ion was determined using the curve-fitting and modeling program, CRUNCH, developed by Armentrout and co-workers[35]

$$\sigma(E) = \sigma_0 \Sigma g_i (E + E_i - E_0)^n/E \quad (2)$$

where $\sigma(E)$ is the dissociation cross-section, σ_0 is a scaling factor, E is the center-of-mass collision energy (E_{cm}), E_0 is the threshold energy, E_i is the internal energy of a given vibrational state with a relative population g_i, and n is an adjustable parameter. An inherent assumption in the use of eq 2 is that a precursor ion with an internal energy greater than E_0 will fragment to form the product ion in q2. With increasing complexity of the precursor ion, there is an increasing probability that the fragmentation reaction will not occur within the precursor ion's residence time in q2. For a relatively large precursor ion that has many degrees of freedom (such as the ones being examined here), additional internal energy is needed to increase the fragmentation rate to a magnitude that the dissociation in q2 becomes measurable. This additional internal energy, the kinetic shift, must be subtracted from the apparent threshold to yield the true E_0. The magnitude of this additional energy can be estimated from the unimolecular rate constant of the dissociation according to the Rice−Ramsperger−Kassel−Marcus (RRKM) theory.[36] When this is done, eq 2 is modified to become

$$\sigma(E) = \sigma_0 \Sigma g_i P(E, E_i, t)(E + E_i - E_0)^n/E \quad (3)$$

where P is the probability that a precursor ion of collision energy E and internal energy E_i will fragment within a residence time of t. As the ion residence time is a function of E, this is evaluated in the model for every experimental collision energy. In comparison with our former approach in using a fixed residence time,[32] this energy-dependent residence time approach resulted in a decrease of 0.02−0.04 eV in E_0 for the ions studied here.

Determination of E_0 requires the vibrational frequencies and rotational constants of the precursor ions and the transitions states. These were obtained from the DFT calculations described in the previous section; the values are given in Table 1S in the Supporting Information section. Altering the vibrational frequencies of both the precursor ions and the transition states systematically by ±10% resulted in a change of the E_0 (u_f) by ±0.02−0.05 eV. This means minor errors in the vibrational frequencies are inconsequential.

Table 2. Threshold Energies and $\Delta H^{\ddagger}_0$ Values

reaction	E_0, eV	E_0 (k.s.), eV	$\Delta H^{\ddagger}_0$ (expt.), kcal/mol	$\Delta H^{\ddagger}_0$ (theory), kcal/mol
$G_3 \rightarrow b_2$	2.81	1.37 (+0.10/−0.12)	31.6 (+2.3/−2.8)	32.3
$b_2 \rightarrow a_2$	1.72	1.45 (+0.08/−0.13)	33.4 (+1.8/−3.0)	32.9
$b_2 \rightarrow a_1$	2.40	1.85 (+0.09/−0.13)	42.7 (+2.1/−3.0)	41.5
		1.69[a] (+0.08/−0.12)	39.0[a] (+1.8/−2.8)	
$a_2 \rightarrow a_1$	1.73	1.48 (+0.08/−0.09)	34.1 (+1.8/−2.1)	35.7

[a] In competition with $b_2 \rightarrow a_2$.

The dissociation cross-sections of the product ions were determined as a function of the center-of-mass energies at four argon pressures, typically at CGT values of 100, 75, 50, and 25 × 10^{12} atoms cm^{-2}. An ion that has a collision cross-section of 100 $Å^2$ will have, on average, undergone one collision in q2 with argon having a CGT value of 100 × 10^{12} atoms cm^{-2}. To eliminate the effects of multiple collisions, E_0 values were obtained from threshold curves constructed only from $\sigma(E)$ at zero CGT. These cross-sections were obtained by extrapolating the $\sigma(E)$ versus CGT function to zero CGT via the least-squares fit of the presumed exponential function.[32] A typical threshold curve in our work comprises 70−90 $\sigma(E)$ values over an E_{cm} range of 0−4 eV.

Ion energy distributions in the laboratory frame of approximately 2 eV (full width at half-maximum) were observed for all ion complexes. These values are practically identical to those observed in earlier studies[32] and are comparable to the best results seen on similar instrumentation.[27] Evaluation of E_0 took into account of the ion energy distribution[37] and the thermal motion of argon.[37,38] These details had been discussed elsewhere.[32] We assume the ion and the argon temperatures to be 298 K. Possible errors due to uncertainty of the ion and argon temperatures were estimated in the following manner. Assuming that the ion temperature falls within 298 ± 100 K and the argon temperature cannot be lower than 198 K, the possible errors in E_0 due to uncertainty in temperatures (u_T) were determined by modeling E_0 at three sets of conditions: (a) ion temperature = argon temperature = 298 K (standard); (b) ion temperature = 398 K, argon temperature = 298 K (high); and (c) ion temperature = argon temperature = 198 K (low). Ions sampled are heated collisionally and cooled by expansion via cryogenic pumping; cooling of argon is possible because of cryogenic pumping. u_T ranges from +0.02 to +0.09 eV and from −0.07 to −0.15 eV, depending on the size of the ion. The smaller positive uncertainties are due in part to a consideration of an increase in only the ion temperature; by contrast, the larger negative uncertainties involve that of a decrease in both the ion and the argon temperatures.

In addition to uncertainty in vibrational frequencies (u_f) as well as that in ion and neutral temperatures (u_T), contributions to the error of E_0 from uncertainties of the flight distance or residence time (u_{fd}) and kinetic shift (u_{ks}) were also accounted for. We estimated that the former would result in an error in E_0 of ±0.02 eV and the latter an error of ±0.1 eV. The total uncertainty of a given E_0 determination after kinetic shift modeling is $u_{total}' = (uf^2 + u_T^2 + u_{fd}^2 + u_{ks})^{0.5}$. As the positive and negative uncertainties are different in u_f and u_T, the positive and negative uncertainties in u_{total}' were propagated separately. The E_0 value for each fragmentation reaction considered was determined in duplicate; the uncertainty in the average was determined by propagating the two u_{total}' as $u_{total} = [(u_{total}'(1))^2 + (u_{total}'(2))^2]^{0.5}/2$. Table 2 lists the E_0 values before and after kinetic shift modeling (E_0 and E_0 (k.s.) plus the $+u_{total}$ and $-u_{total}$ values in parentheses.

(33) (a) Douglas, D. J. *J. Phys. Chem.* **1982**, *86*, 185−191. (b) Douglas, D. J.; French, J. B. *J. Am. Soc. Mass Spectrom.* **1992**, *3*, 398−408. (c) Covey, T.; Douglas, D. J. *J. Am. Soc. Mass Spectrom.* **1993**, *4*, 616−623. (d) Goeringer. D. E.; Asano, K. G.; McLuckey, S. A. *Int. J. Mass Spectrom.* **1999**, *182/183*, 275−288. (e) Asano, K. G.; Goeringer, D. E.; McLuckey, S. A. *Int. J. Mass Spectrom.* **1999**, *185/186/187*, 207−219. (f) Drahos, L.; Heeren, R. M. A.; Collette, C.; De Pauw, E.; Vékey, K. *J. Mass Spectrom.* **1999**, *34*, 1373−1379. (g) Schneider, B. B.; Chen, D. D. Y. *Anal. Chem.* **2000**, *72*, 791−799. (h) Schneider, B. B.; Douglas, D. J.; Chen, D. D. Y. *J. Am. Soc. Mass Spectrom.* **2001**, *12*, 772−779.

(34) Dawson, P. H.; French, J. B.; Buckley, J. A.; Douglas, D. J.; Simmons, D. *Org. Mass Spectrom.* **1982**, *17*, 205−211.

(35) (a) Ervin, K. M.; Armentrout, P. B. *J. Chem. Phys.* **1985**, *83*, 166−189. (b) Weber, M. E.; Elkind, J. L.; Armentrout, P. B. *J. Chem. Phys.* **1986**, *84*, 1521−1529. (c) Schultz, R. H.; Crellin, K. C.; Armentrout, P. B. *J. Am. Chem. Soc.* **1991**, *113*, 8590−8601. (d) Dalleska, N. F.; Honma, K.; Sunderlin, L. S.; Armentrout, P. B. *J. Am. Chem. Soc.* **1994**, *116*, 3519−3528. (e) Shvartsburg, A. A.; Ervin, K. M.; Frederick, J. H.; *J. Chem. Phys.* **1996**, *104*, 8458−8469. (f) Rodgers, M. T.; Ervin, K. M.; Armentrout, P. B. *J. Chem. Phys.* **1997**, *106*, 4499−4508. (g) Rodgers, M. T.; Armentrout, P. B. *J. Chem. Phys.* **1998**, *109*, 1787−1800.

(36) (a) Gilbert, R. G.; Smith, S. C. *Theory of Unimolecular and Recombination Reactions*: Blackwell Scientific Publications: Oxford, 1990. (b) Truhlar, D. G.; Garrett, B. C.; Klippenstein, S. J. *J. Phys. Chem.* **1996**, *100*, 12 771−12 800. (c) Holbrook, K. A.; Pilling, M. J.; Robertson, S. H. *Unimolecular Reactions*, 2nd ed.; Wiley: New York, 1996.

(37) Lifshitz, C.; Wu, R. L. C.; Tiernan, T. O.; Terwilliger, D. T. *J. Chem. Phys.* **1978**, *68*, 247−260.

(38) Chantry, P. J. *J. Chem. Phys.* **1971**, *55*, 2746−2759.

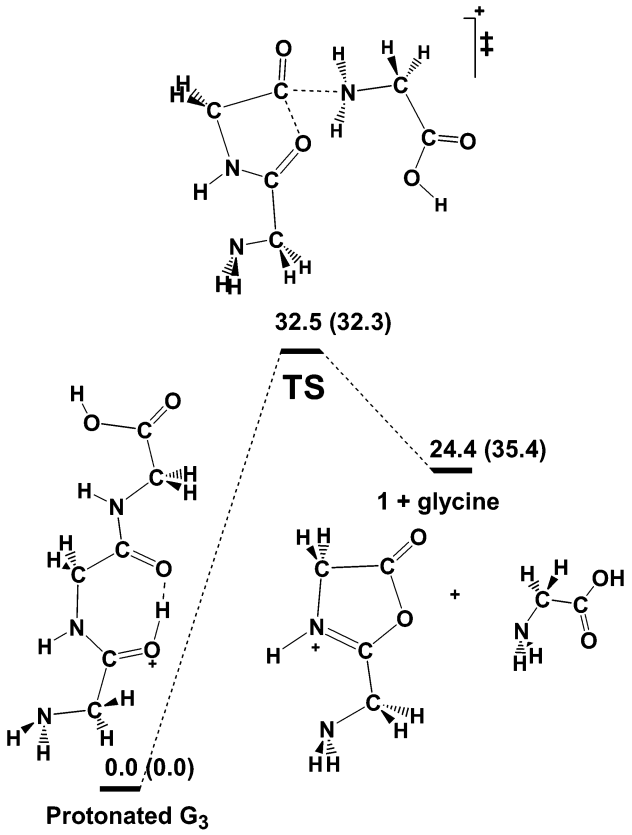

Figure 1. Simplified energy profile for the fragmentation of protonated triglycine to the b_2 ion and glycine: first values are $\Delta G°_{298}$; values in parentheses are $\Delta H°_0$.

Threshold CID is most commonly applied to measuring binding enthalpies of metal ions (M^+) to ligands (L). The E_0 of the reaction $M^+-L \rightarrow M^+ + L$ gives the enthalpy change of the reaction at 0 K, $\Delta H°_0$, the binding energy. An inherent assumption in equating E_0 to $\Delta H°_0$ is that the dissociation is barrierless, which applies to the dissociation of most metal−ligand complexes, where L contains only one metal-binding site. Rearrangement reactions, including the dissociation reactions that are examined in this study, have significant barriers. For these reactions, the E_0 values are measures of the barrier heights in terms of enthalpies at 0 K or $\Delta H^{\ddagger}_0$ (vide infra). Table 2 also lists the $\Delta H^{\ddagger}_0$ in terms of kcal/mol with positive and negative uncertainties in parentheses.

Results and Discussion

Fragmentation of Protonated G_3 to the b_2 Ion. As mentioned earlier, a recent study of ours has established that in collisionally activated protonated triglycine, it is indeed energetically feasible for the proton to migrate from its original position on the N-terminal amino nitrogen atom, through a number of tautomeric intermediates, to the amide nitrogen of the second peptide linkage.[5] After the last migration step, the carbonyl oxygen atom of the first amide bond attacks the carbonyl carbon of the second amide bond, thereby forming a transition state comprised of an incipient oxazolone (the b_2 ion) and an incipient (neutral) glycine. The products then separate to give the b_2 ion, **1**, and glycine. A simplified version of the energy profile (showing only the key step) is shown in Figure 1. The reader is referred to Figure 2 in Reference 5 for the complete energy profile. The barrier shown in Figure 1 has a free energy value at 298 K of 32.5 kcal/mol.[5] For the purpose of this study the critical barrier height in terms of enthalpy at

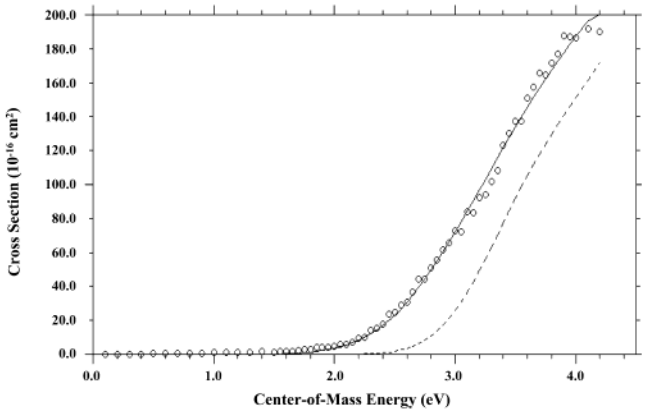

Figure 2. Threshold curve for the fragmentation of protonated triglycine to the b_2 ion at modeled ion and argon temperatures of 298 K: ○, experimental data; full line, best fit to the experimental data; dashed line, modeled cross-section at 0 K.

0 K, $\Delta H^{\ddagger}_0$ (shown in parentheses), is more relevant, as it is this value that is measured in the threshold CID experiments. This $\Delta H^{\ddagger}_0$ value is 32.3 kcal/mol. Note that the products are lower in free energy but higher in enthalpy than the transition state, thereby demonstrating the importance of considering free energy in rearrangement reactions.

Experimental E_0 values for the fragmentation of protonated G_3 to the b_2 ion are shown in Table 2, along with those for the fragmentation of b_2 to a_2, b_2 to a_1, and a_2 to a_1. Figure 2 shows a zero-CGT threshold curve for the dissociation of G_3 to b_2. Converting the E_0 values that incorporate the kinetic shifts (E_0 (k.s.)) to units of kcal/mol gives experimental $\Delta H^{\ddagger}_0$ ($\Delta H^{\ddagger}_0$ (expt.)). For the fragmentation of G_3 to b_2, the $\Delta H^{\ddagger}_0$ (expt.) value of 31.6 (+2.3/−2.8) kcal/mol is in good agreement with the B3LYP/6-31++G(d,p) $\Delta H^{\ddagger}_0$ value of 32.3 kcal/mol.[5] DFT calculations at this level of theory have been found to deviate typically from the best experimental values by no more than 2−3 kcal/mol.[39] The agreement between the experimental and calculated $\Delta H^{\ddagger}_0$ values lends credence to the published mechanism[5] as well as to the experimental approach in this study.

Fragmentation of the b_2 to the a_2 Ion. Harrison's group[7a,b] proposed that the fragmentation of b_2 to a_2 proceeds via a "reacting configuration" that is the acylium ion. They supported their proposal with kinetic energy release ($T_{1/2}$) measurements that show relatively large values of 0.44−0.53 eV, which is consistent with a transition state that lies considerably above the final products in energy.

Figure 3 shows the reaction profile in terms of $\Delta G°_{298}$ calculated in this study at the B3LYP/6-31++G(d,p) level of theory that contains elements of Harrison's[7a,b] proposal and a more recent proposal by Paizs et al.[40] Corresponding $\Delta H°_0$ values are shown in parentheses. Simplified structures of the stationary points are shown; the readers are referred to Figure 1S in the Supporting Information section for the detailed structures. The C−O bond in **1**, protonated 2-aminomethyl-5-oxazolone, is relatively weak and has a calculated distance of

(39) (a) Wang, Z.; Chu, I. K.; Rodriquez, C. F.; Hopkinson, A. C.; Siu, K. W. M. *J. Phys. Chem. A* **1999**, *103*, 8700−8705. (b) Rodriquez, C. F.; Shoeib, T.; Chu, I. K.; Siu, K. W. M.; Hopkinson, A. C. *J. Phys. Chem. A* **2000**, *104*, 5335−5342. (c) Addario, V.; Guo, Y.; Chu, I. K.; Ling, Y.; Ruggerio, G.; Rodriquez, C. F.; Hopkinson, A. C.; Siu, K. W. M. *Int. J. Mass Spectrom.* **2002**, *219*, 101−114.

(40) Paizs, B.; Szlávik, Z.; Lendvay, G.; Vékey, K.; Suhai, S. *Rapid Commun. Mass Spectrom.* **2000**, *14*, 746−755.

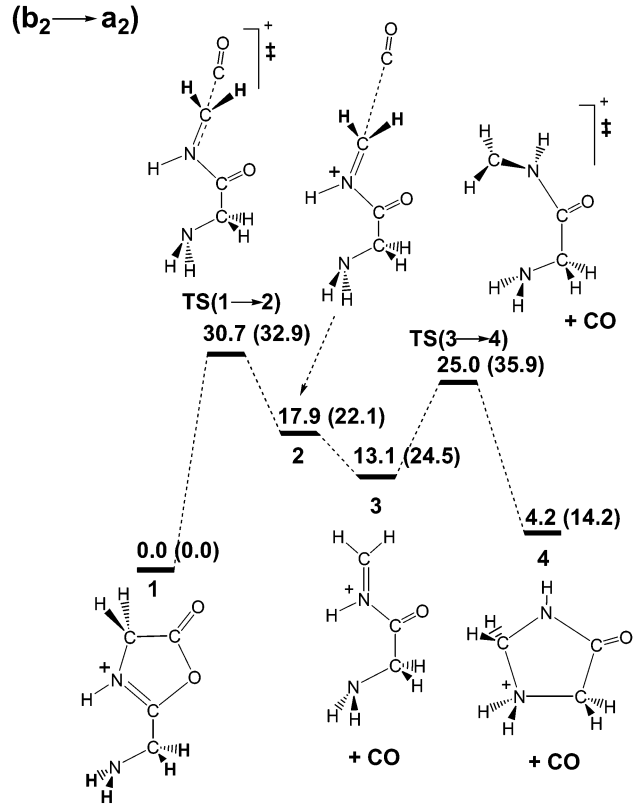

Figure 3. Reaction profile for the fragmentation of the b_2 to the a_2 ion: first values are ΔG°_{298}; values in parentheses are ΔH°_0.

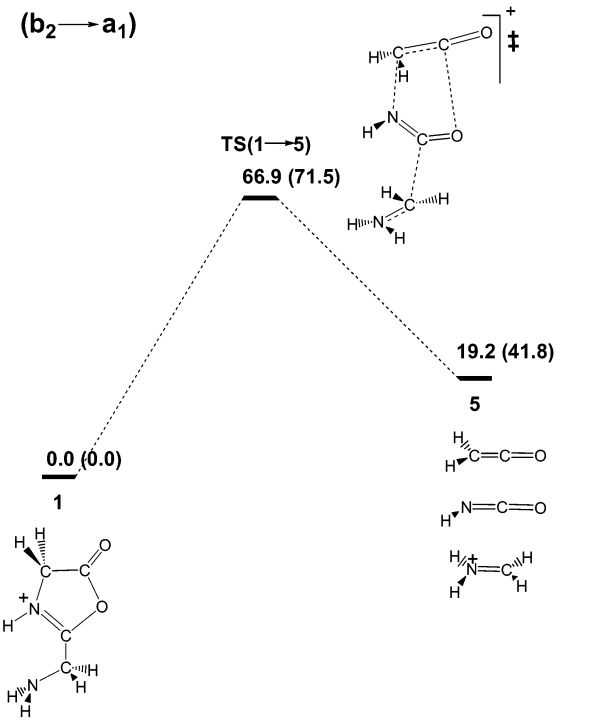

Figure 4. High critical energy fragmentation of the b_2 to the a_1 ion: first values are ΔG°_{298}; values in parentheses are ΔH°_0.

1.480 Å (Figure 1S). Cleavage of the C−O bond opens the five-membered ring to produce structure **2** via transition structure **TS(1→2)**. The activation energy in terms of ΔG°_{298} for this process is 30.7 kcal/mol. The terminal CO in both structure **2** and transition structure **TS(1→2)** is loosely attached as witnessed by the long C−C distances (2.985 and 1.826 Å, respectively). Structure **2** is the classical acylium ion structure that has long been discussed in the literature.[6] It lies 17.9 kcal/mol in free energy above **1** and is, in reality, an ion−neutral complex consisting of the classical a_2 ion solvated by CO. The loss of CO from **2** is exoergic by 4.8 kcal/mol and endothermic by 2.4 kcal/mol. The product ion **3**, the iminium or immonium ion, has long been proposed as the structure for the *a* ions.[6] The combination of **3** and CO is 13.1 kcal/mol higher in free energy than the b_2 ion, **1**. The iminium ion **3** is, however, not the lowest energy structure on the a_2 ion free energy surface. Nucleophilic attack by the terminal amino group on the methylene carbon at the other terminus (**TS(3→4)**) results in the five-membered ring structure **4**. As far as we know, structure **4**, protonated 4-imidazolidone, has never been proposed as a possible a_2 structure. Protonated 4-imidazolidone lies 8.9 kcal/mol below the iminium ion in free energy; the combination of protonated 4-imidazolidone and carbon monoxide is only 4.2 kcal/mol higher in free energy than the b_2 ion, protonated 2-aminomethyl-5-oxazolone (Figure 3).

The rate-determining step in the fragmentation of b_2 to a_2 at 298 K is the opening of the oxazolone ring via **TS(1→2)** to form the iminium ion solvated by CO. It may be of note that **TS(3→4)** is lower in relative free energy albeit higher in relative enthalpy. **TS(1→2)** lies 30.7 kcal/mol in free energy above **1**; in terms of enthalpy ($\Delta H^\ddagger_0$ (theory)), it is 32.9 kcal/mol. The $\Delta H^\ddagger_0$ (expt.) is 33.4 (+1.8/-3.0) kcal/mol (Table 2). The good agreement between the experimental and calculated $\Delta H^\ddagger_0$ supports the proposed reaction profile shown in Figure 3. Furthermore, the reverse activation barrier (between **TS(1→2)** and **4** + CO), at 26.5 kcal/mol in free energy, is considerable and is in accordance with the relatively large $T_{1/2}$ observed by the Harrison group.[7a]

Fragmentation of the b_2 to the a_1 Ion. Experimentally, fragmentation of the b_2 ion can yield the a_1 ion directly or indirectly via the a_2 ion. The proof for direct a_1 formation is that this product ion is produced near threshold conditions under single-collision conditions and that the sum of the threshold energies for the dissociations of b_2 to a_2 and a_2 to a_1 exceeds the threshold for the direct dissociation of b_2 to a_1 (Table 2). A mechanism for the direct dissociation of b_2 to a_1 has been postulated.[12] For the b_2 from G_3, the postulated products are the a_1 ion ($H_2N^+{=}CH_2$), CH_2CO, and HNCO.[12] This was the first fragmentation mechanism that we investigated; the transition state structure, **TS(1→5)**, that results (Figure 4), however, is 66.9 kcal/mol above **1** in free energy, a value much too high to be compatible with the experimental results. Furthermore, the reverse activation barrier is 47.7 kcal/mol in free energy, which is excessive in light of the relatively small $T_{1/2}$ reported for phenylalanylglycylglycine.[12] The reaction profile of a mechanism that agrees with the threshold CID data is shown in Figure 5. As before, ΔG°_{298} data are shown with the corresponding ΔH°_0 values in parentheses.

Collisional activation of **1**, protonated 2-aminomethyl-5-oxazolone, results in extension of the exocyclic C−C bond to form **TS(1→6)**, which may be viewed as an activated complex between the incipient a_1 ion and an incipient carbene. This transition state lies 39.3 kcal/mol in terms of free energy above **1**. However, the lowest energy pathway to the a_1 ion is not one that involves separation of the two incipient structures to form

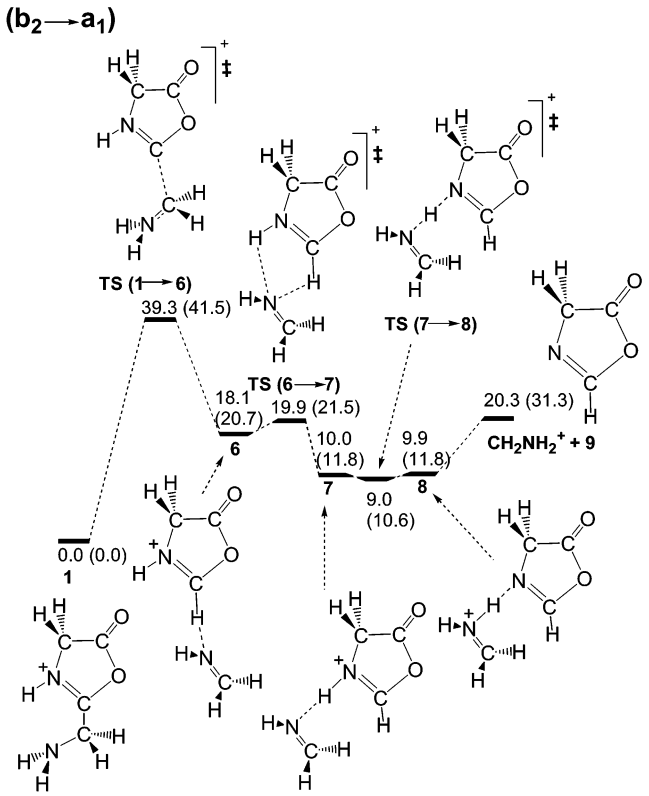

Figure 5. Reaction profile for the fragmentation of the b_2 to the a_1 ion: first values are $\Delta G°_{298}$; values in parentheses are $\Delta H°_0$.

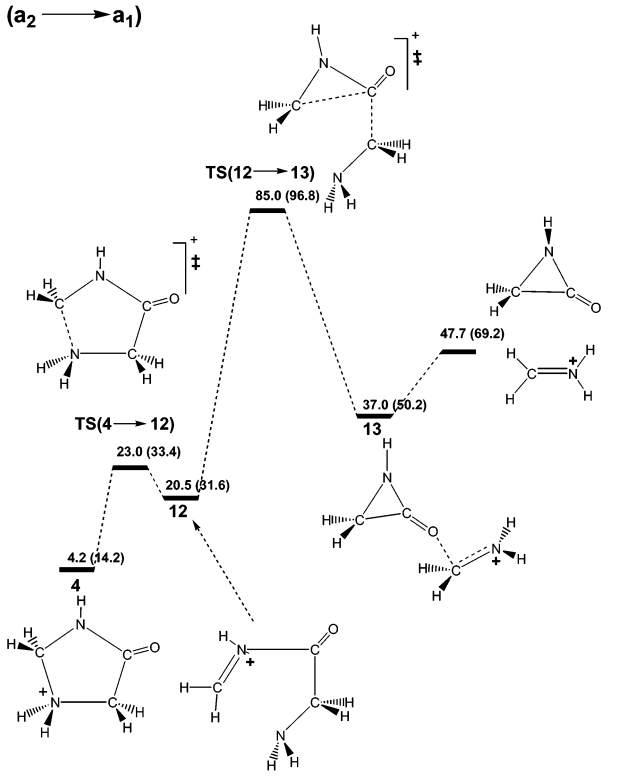

Figure 6. High critical energy fragmentation of the a_2 to the a_1 ion: first values are $\Delta G°_{298}$; values in parentheses are $\Delta H°_0$.

the a_1 ion and the neutral carbene, **11**; these separated products lie 47.4 kcal/mol above **1** (Table 1). Instead, at or near threshold conditions, a_1 is formed via a number of low-energy rearrangement reactions that take place within the ion−neutral complex. The minimum on the product side of **TS(1→6)**, as determined by an intrinsic reaction coordinate calculation is **6**, an ion neutral complex between protonated oxazolone, **10**, and methanimine. The methanimine then slides over and hydrogen bonds with the N−H proton of the protonated oxazolone to form complex **7**. Transfer of hydrogen across to the methanimine results in complex **8**. [It is noteworthy that **TS(7→8)** is lower in free energy and enthalpy than both structures **7** and **8**. The total electronic energy, E_t, of **TS(7→8)** is slightly larger than those of structures **7** and **8** (Table 1). However, addition of zero-point vibrational energies makes the $\Delta H°_0$ value of **TS(7→8)** smaller than the $\Delta H°_0$ values of **7** and **8**, because the imaginary frequency mode of **TS(7→8)** does not contribute, whereas all vibrational modes in structures **7** and **8** are real and do contribute.] Subsequent cleavage of the hydrogen bond yields the iminium ion, a_1, and oxazolone, **9**. The separated products lie only 20.3 kcal/mol in free energy above **1**. The rate-determining step is the formation of **TS(1→6)**, for which the computed $\Delta H^{\ddagger}_0$ value is 41.5 kcal/mol.

Table 2 shows two $\Delta H^{\ddagger}_0$ (expt.) values. The larger value of 42.7 (+2.1/−3.0) kcal/mol was obtained by considering the b_2 to a_1 fragmentation on its own. The smaller value of 39.0 (+1.8/−2.8) kcal/mol was obtained by considering the reaction to be in competition with the b_2 to a_2 fragmentation, which has a comparatively lower threshold energy (Table 2). Studies by Rodgers and Armentrout, and DeTuri and Ervin[41] have shown that the competitive modeling produces better thermodynamic values for bond dissociation energies of lithiated complexes and gas-phase acidities of alcohols. The $\Delta H^{\ddagger}_0$ (theory) value of 41.5 kcal/mol is between the two $\Delta H^{\ddagger}_0$ (expt.) values. We expect typical errors of B3LYP/6-31++G(d,p) calculations for the type of molecules in question to be about 2 to 3 kcal/mol;[39] thus, both $\Delta H^{\ddagger}_0$ (expt.) values are within the estimated error limits of the $\Delta H^{\ddagger}_0$ (theory). As before, agreement between the experimental and calculated $\Delta H^{\ddagger}_0$ lends support to the proposed mechanism shown in Figure 5. It is noteworthy that the reverse barrier (between **TS(1→6)** and a_1 + **9**) is relatively small at 19.0 kcal/mol in terms of free energy. This value is much smaller than that in the originally postulated mechanism, which has a value of 47.7 kcal/mol, and is more in line with the relatively small $T_{1/2}$ reported, albeit for phenylalanylglycylglycine.[12]

Fragmentation of the a_2 to the a_1 Ion. No mechanism for the fragmentation of a_2 to a_1 has previously been proposed. However, a mechanism for the formation of internal iminium ions in which the neutral product that accompanies the internal iminium ion is an aziridinone has been forwarded.[12] The aziridinone is a frequently mentioned neutral product in peptide fragmentation. It is the proposed neutral product in the fragmentation of G_3 to y_2,[7c] despite the fact that it is highly strained and comparatively high in energy ($\Delta G°_{298}$ = 22.0 kcal/mol) versus the isobaric neutral equivalents of methanimine and CO.

For the fragmentation of a_2 to a_1, we first investigated the mechanism that has the aziridinone as the neutral product. The reaction profile is shown in Figure 6. Opening of protonated

(41) (a) Rodgers, M. T.; Armentrout, P. B. *J. Chem. Phys.* **1998**, *109*, 1787−1800. (b) DeTuri, V. F.; Ervin, K. M. *J. Phys. Chem. A* **1999**, *103*, 6911−6920.

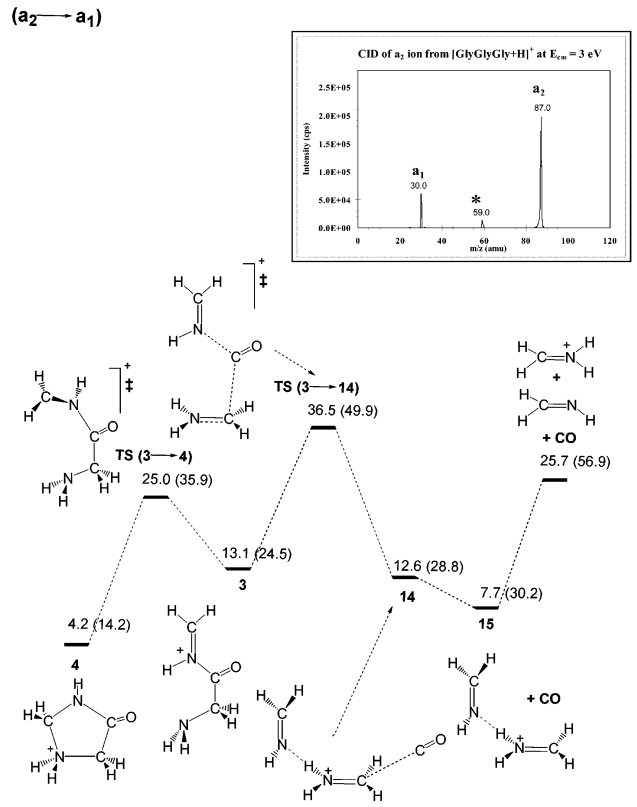

Figure 7. Reaction profile for the fragmentation of the a_2 to the a_1 ion: first values are ΔG°_{298}; values in parentheses are ΔH°_0.

4-imidazolidone, **4**, produces the iminium ion, **12**, a rotamer of **3**. Lengthening of the C−C distance concomitantly with shortening the C- - -C distance results in **TS(12→13)**, the product of which is **13**, a complex between the a_1 ion and aziridinone. These components then separate and yield the products. **TS-(12→13)** lies 80.8 kcal/mol in free energy above **4** and thus is associated with much too high a critical energy for this mechanism to be feasible. As G_3 comprises only glycyl residues, its a_1 ion is identical to its internal iminium ion, whose proposed coproduct is the aziridinone.[12] However, the activation barrier for that mechanism (not shown) at 65 kcal/mol is also too high.

The reaction profile that fits the experimental data is shown in Figure 7. Collisional activation of protonated 4-imidazolidone, **4**, yields the iminium ion, **3**. The C−C and C−N bonds adjacent to the carbonyl group then lengthen simultaneously, producing **TS(3→14)**. This is the critical step in the dissociation and **TS-(3→14)** lies only 32.3 kcal/mol above **4** in terms of free energy at 298 K. The other minimum associated with this transition state is **14**, best described as an adduct between an iminium-imine complex and CO. The CO is very weakly held in **14**; the OC····C bond is very long at 3.213 Å. In comparison, the N····H hydrogen bond between the imine and the iminium ion is shorter at 1.564 Å and presumably stronger (Figure 1S). Dissociation of **14** to **15**, the iminium-imine complex, and CO is exoergic by 4.9 kcal/mol and endothermic by 1.4 kcal/mol. Dissociation of **15** yields the a_1 ion and methanimine; the separated products lie 21.5 kcal/mol above **4** in free energy at 298 K. Significantly, there is experimental support for the existence of structure **15**; the inset in Figure 7 shows the product-ion spectrum of the a_2 ion at a center-of-mass energy of 3 eV. The iminium-imine complex (structure **15**), if it survives collisional activation, should have an *m*/*z* value of 59.0 Th and, indeed, the only other fragment ion observed in the product-ion spectrum of a_2 occurs at this *m*/*z* value. The existence of the iminium-imine complex immediately suggests a mechanism whereby an internal iminium ion may be formed. The internal iminium ion is distinguishable from the a_1 ion in peptides whose first and second residues are different. This mechanism and its consequences will be the subject of a future report.

As discussed earlier, the rate-determining step at 298 K in the fragmentation of the a_2 to the a_1 ion is the formation of **TS(3→14)**. The $\Delta H^\ddagger_0$ (expt.) value determined is 34.1 (+1.8/−2.1) kcal/mol, in good agreement with the $\Delta H^\ddagger_0$ (theory) value of 35.7 kcal/mol (Table 2).

Conclusions

The combination of threshold CID measurements and DFT has enabled us to discover novel mechanisms and structures, and to confirm proposed ones, in the fragmentation of peptide-derived ions. The dissociation of the b_2 ion of G_3 to a_2 does indeed proceed via a transition state that is acylium-like; a novel a_2 ion structure, the protonated 4-imidazolidone, however, is proposed. For G_3-derived ions, this cyclic a_2 structure is lower by 8.9 kcal/mol in free energy than the classical, iminium ion structure. The dissociation of b_2 to a_1 proceeds via a critical transition state that resembles an ion−neutral complex between an incipient a_1 ion and an incipient carbene; the neutral coproduct in the formation of a_1 is an oxazolone. The fragmentation of a_2 to a_1 proceeds via a critical activated complex that comprises three incipient components: an a_1 ion, CO and an imine. Good agreement between measured and theoretical barriers was used as the critical criterion in judging competing mechanisms.

Acknowledgment. We thank Professor P. B. Armentrout for making his CRUNCH program available to us. We would like to thank him, Professors M.T. Rodgers, A.G. Harrison, and P. Kebarle for helpful discussions regarding various aspects of this work, which was generously supported by the Natural Science and Engineering Research Council of Canada (NSERC), MDS SCIEX, the Canadian Foundation of Innovation (CFI), the Ontario Innovation Trust (OIT), and York University. Efforts by Dr. Galina Orlova and Ms. Noah Nour on computation that arose during the revision stage were much appreciated.

Supporting Information Available: Table 1S: Vibrational frequencies and rotational constants of the precursor ions and transition states. Figure 1S: Detailed structures of ions and neutrals. This material is available free of charge via the Internet at http://pubs.acs.org.

JA0207293